In Vivo Prediction of Tuberculosis-Associated Cavity Formation in Rabbits

Brian Luna,[1,a] André Kubler,[1,6,a] Christer Larsson,[1,b] Brent Foster,[4] Ulas Bagci,[4] Daniel J. Mollura,[4] Sanjay K. Jain,[1,2,3] and William R. Bishai[1,2,5]

[1]Johns Hopkins Center for Tuberculosis Research, [2]Center for Infection and Inflammation Imaging Research, [3]Department of Pediatrics, Johns Hopkins University School of Medicine, Baltimore, [4]Center for Infectious Disease Imaging, Department of Radiology and Imaging Sciences, National Institutes of Health, Bethesda, and [5]Howard Hughes Medical Institute, Chevy Chase, Maryland; and [6]Department of Medicine, Imperial College London, United Kingdom

The presence of cavitary lesions in patients with tuberculosis poses a significant clinical concern due to the risk of infectivity and the risk of antibiotic treatment failure. We describe 2 algorithms that use noninvasive positron emission tomography (PET) and computed tomography (CT) to predict the development of cavitary lesions in rabbits. Analysis of the PET region of interest predicted cavitary disease with 100% sensitivity and 76% specificity, and analysis of the CT region of interest predicted cavitary disease with 83.3% sensitivity and 76.9% specificity. Our results show that restricting our analysis to regions with high [^{18}F]-fluorodeoxyglucose uptake provided the best combination of sensitivity and specificity.

Keywords. CT; [^{18}F]-FDG; PET; tuberculosis.

Mycobacterium tuberculosis is the primary etiological agent of tuberculosis in humans and was responsible for an estimated 1.4 million deaths in 2011 [1]. The initial infection is usually cleared or otherwise contained by the host immune system in a granuloma. One hypothesis is that cavities evolve when solid caseous necrotic granulomas liquefy [2]. Cavities are a risk factor for disease transmission [3]. The tissue destruction that results from cavitation contributes to the morbidity and mortality of tuberculosis [2, 4, 5]. Cavitary disease is also an indicator of treatment failure and disease relapse [6].

There are no clinical tests that are designed to assay the risk of cavitary lesion development [7]. Imaging markers provide an attractive option because of their benefit of providing a real-time, noninvasive tool. Additionally, noninvasive imaging tests allow for monitoring disease progression within a patient over time.

We used a rabbit cavitary model of tuberculosis to develop imaging markers predictive of cavitary lesion development. In this study, we demonstrate that, although inflammation, as measured by [^{18}F]-fluorodeoxyglucose ([^{18}F]-FDG) uptake, does not positively correlate with cavitary disease, changes in lung density, as measured by CT, are predictive of cavitary lesion development. We believe this novel method can be used as a noninvasive tool to analyze the progression of tuberculosis cavitary lesions. Such imaging biomarkers could shorten the time and cost of tuberculosis drug trials and are valuable in evaluating therapeutics that target the cavitation process.

MATERIALS AND METHODS

Ethics Statement

All animal experiments were performed in strict accordance with the recommendations in the Guide for the Care and Use of Laboratory Animals of the National Institutes of Health, and all procedures were approved by the Johns Hopkins University Animal Care and Use Committee.

Modified Rabbit Cavitary Model

Sensitization and infection of New Zealand White female rabbits were done as previously described [8]. Briefly, rabbits received 5 separate injections of 10^8 colony-forming units (CFUs) of heat-killed *Mycobacterium bovis* Ravenel. Twenty-five days after the final injection, the animals were given a skin test (purified protein derivative) to measure hypersensitivity. Positivity was defined as any measurable induration. Animals for which the skin test revealed no conversion were still included in this study. Following receipt of the skin test results, rabbits were challenged with 10^4 live *M. tuberculosis* H37Rv bacilli. The bacterial suspension was delivered to the right lower lung lobe by bronchoscopy. Inoculum dose was determined by plating the inoculum on 7H11 selective plates.

[^{18}F]-FDG PET/CT Imaging

Rabbits were anesthetized with ketamine (20 mg/kg), xylazine (5 mg/kg), and acepromazine (10 mg). Animals were maintained under 3 L/min O_2 and 1% isoflurane for the duration

Received 14 April 2014; accepted 31 July 2014; electronically published 12 August 2014.

[a]B. L. and A. K. contributed equally to this work.

[b]Present affiliation: Department of Molecular Biology, Umeå University, Sweden.

Correspondence: William R. Bishai, MD, PhD, Johns Hopkins Center for Tuberculosis Research, Johns Hopkins School of Medicine, 1550 Orleans, CRB2 St, Ste 103, Baltimore, MD 21231 (wbishai@jhmi.edu).

The Journal of Infectious Diseases® 2015;211:481–5

DOI: 10.1093/infdis/jiu449

of the imaging. Because the imaging facility is located in a biosafety level 2 facility, the infected animals were placed into a biosafety imaging chamber (Mediso). This chamber allowed for the filtration of gas exchange and for the safe transport of the animal. A total of 2 mCi of [^{18}F]-FDG was administered into the marginal ear vein. PET images were acquired on a Philips Mosaic PET scanner. Forty-five minutes after injection, PET data were acquired by a 30-minute static scan. CT images were obtained with a clinical 8-slice CereTom CT (NeuroLogica) scanner.

Imaging Processing, Segmentation, Coregistration, and Regions of Interest (ROIs)

An overview of the image processing is summarized in Supplementary Figure 1. Fiducial markers were used to coregister PET images to the CT images. A group of 5 thin-walled polymerase chain reaction (PCR) tubes containing 5 μCi of [^{18}F]-FDG were used as the fiducial markers. Rigid image coregistration was done using AMIRA (Visualization Science Group). Image segmentation was done using both AMIRA and the ANNOTATION TOOL (National Institutes of Health) software packages. Methods for image segmentation accorded with those described by Bagci et al [9]. Briefly, lung segmentation was conducted by an adaptive region growing algorithm in which the user-defined voxels were labeled as "lung" or "nonlung" regions [10]. Explicitly labeled voxels are used to determine the status of the unlabeled voxels. Furthermore, manual interaction for refinement of dense pathological regions within the lung was also possible, using the brush tools or random walk region segmentation algorithm [9, 11]. The segmented lung regions were then converted into binary masks such that nonlung regions were removed from the raw images. PET ROIs were defined by thresholding the top fifth percentile of [^{18}F]-FDG uptake. CT ROIs were defined as being between −200 and 200 Hounsfield units (HU).

Statistical Analyses

Statistical analysis was done using PRISM (GraphPad Software). For analysis that consisted of comparing multiple time points, statistical significance was determined by a repeated-measures 1-way analysis of variance with a Bonferroni multiple comparison test. For pairwise analysis, a 2-tailed, unpaired Student's *t* test was done. *P* values of >.05 were considered nonsignificant.

RESULTS

Rabbit Model of Cavitary Disease Training Set

Twelve rabbits were presensitized and infected with 10^4 CFUs of *M. tuberculosis* H37Rv. Rabbits underwent PET and CT at the following time points: before infection and on days 14, 21, 28, 35, 70, and 140 after infection. In total 114 image sets, comprised of 57 PET and 57 CT data sets, were collected and analyzed. Cavitary progressive disease was defined by visual assessment of a cavity structure during necropsy or observing a region with density of less than −900 HU as measured by CT. Animals in which no cavitary disease was observed were labeled as having noncavitary progressive disease.

PET and CT ROIs

Raw PET and CT images were acquired, coregistered, and then segmented. The PET ROI was defined as a global threshold of the top fifth percentile of [^{18}F]-FDG uptake, and the CT ROI was defined by the density range of −200 to 200 HU. The PET and CT ROIs were applied to the segmented PET and CT data sets, respectively (Supplementary Figure 1). The PET ROI can be summarized as defining a region with high inflammation, and the CT ROI can be summarized as defining a consolidated region. Both regions identify abnormalities that can be interpreted as signs of disease. A summary of the main types of pathology that are visualized by CT are summarized in Figure 1*A*. Because PET and CT images have been coregistered, application of the ROI is not restricted to the data set used to generate the ROI. For example the spatial volume defined by the PET ROI can be applied to the CT image set and also the PET data set.

Changes in Lung Density During Disease Progression

Progression of active tuberculosis in the rabbit model leads to structural changes, such as fibrosis, that can be measured as an increase in lung tissue density (Figure 1*B*). A significant difference ($P = .0038$) was found when comparing the lung density distribution in cavitary progressive animals at the week of cavitation versus the week prior to cavitation (Figure 1*B*). A significant difference was also observed when measuring the density distribution at the week of cavitation, compared with the week prior to cavitation, using the PET ROI (2-tailed unpaired *t* test; Figure 1*C*). The density distribution of cavitary progressing animals did show an increasing trend in the 0:100 HU domain in the CT ROI (Figure 1*D*).

Defining an Imaging Marker of Cavitation

We observed that the shifts in the density distribution from the PET ROI produced a peak in the −200 to 200 HU region (Figure 1*B*–*D*). It was also observed that a significant increase ($P = .0003$) in lung density in range of −200 to 200 HU occurs after infection (Supplementary Figure 2*A*). There was a significant difference ($P = .0001$) between cavitary progressing and noncavitary progressing animals when measuring the percentage of lung within the range of −200 to 200 HU (Supplementary Figure 2*B*).

Assessment of the Predictive Power of the Imaging Markers, Using the Test Set

We developed 2 methods for predicting cavitary lesion progression, using the data we collected from the training set series of

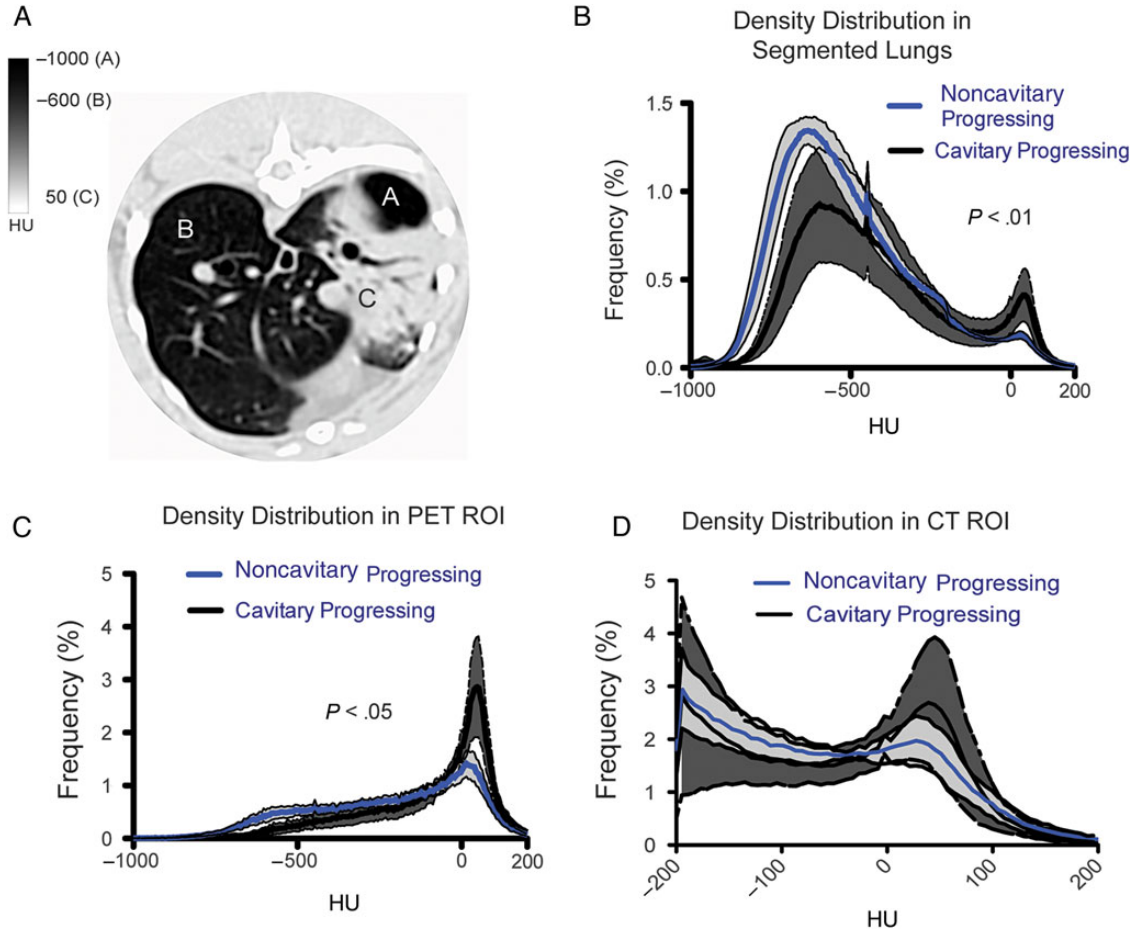

Figure 1. Density change in cavitary progressing and noncavitary progressing groups. Positron emission tomography (PET) and computed tomography (CT) image sets were first coregistered, and the lung field was defined by CT. A binary mask of the CT-defined lung field was then multiplied against the PET image stack to define the lung field in the PET image stack. Subsequent regions of interest (ROIs) were defined by either CT or PET as described below. *A*, A general representation of the densities associated with different disease pathologies observed by CT. "A" represents a cavity, "B" represents normal lung, and "C" represents a region of consolidation. *B*, Density, as measured from the segmented, total lung reconstruction. A significant difference was observed between the 2 groups ($P = .0038$). *C*, Density distribution within the PET ROI. A significant difference was observed between the groups ($P = .038$). *D*, Density distribution within the CT ROI. The cavitary progressing group showed increased density in the 0–100 HU domain.

animals. The methods quantify the density distribution, as measured by CT, using differently defined ROIs. The area under curve (AUC) cutoffs of >90 and >115 for the PET and CT ROIs, respectively, were positive predictors for the development of cavitary disease. These criteria were designed to provide the best combination of both sensitivity and specificity. Images defined as positive were the week of cavitation and the week prior to cavitation. Therefore, the training set consisted of 10 positive imaging sets and 47 negative imaging sets (Table 1).

To validate the usefulness of these methods, these predictive criteria were applied to a new test set of rabbits. The test set was subjected to the same infection conditions as the training set group. Three of 4 animals developed cavitary disease from the test set. The test set was imaged before infection and 1, 2, 3, and 5 weeks after infection and consisted of 6 positive images and 13 negative images (the week 5 image from 1 rabbit was not used because it was obtained 2 weeks after cavitation occurred). Use of the PET ROI predicted cavitary disease with 100% sensitivity

Table 1. Sensitivity and Specificity of Cavitary Predictive Radiology Markers

Marker	Training Set[a]		Test Set[b]	
Region of interest	PET	CT	PET	CT
Area under the curve	90	115	90	115
Sensitivity, %	90	80	100	83.333
Specificity, %	78.182	72.727	76.923	76.923

Use of the PET ROI outperformed the CT ROI.

Abbreviations: CT, computed tomography; PET, positron emission tomography; ROI, regions of interest.

[a] There were 10 true positive and 55 true negatives.

[b] There were 6 true positives and 13 true negatives.

and 76% specificity, and use of the CT ROI predicted cavitary disease with 83.3% sensitivity and 76.9% specificity (Table 1). Cavitary lesions that were identified by PET and CT were consistent with histopathologic findings, as well (Supplementary Figure 3). Cavitary disease was reliably predicted up to 1 week in advance of cavitation.

DISCUSSION

Tuberculosis biomarkers for monitoring disease outcome are urgently needed. The use of imaging biomarkers could have an immediate impact in a clinical trail setting in which resources are more abundant. At present, the cost of clinical trials for new tuberculosis vaccines and drugs is staggeringly high because of poor biomarkers. Identification of robust biomarkers to monitor treatment outcome could dramatically reduce both the financial cost and study duration needed to evaluate new therapeutics [7]. These technologies may also have value in clinical care and management as costs decline. This tool can also be used for reducing the number of animals used for studies and also for mitigating animal suffering. The number of animals used for studies can be reduced because the noninvasive imaging techniques described do not require animals to be euthanized at each time point.

The improved sensitivity of predicting cavitary disease for the PET ROI, compared with the CT ROI, is likely due to a positive correlation between [^{18}F]-FDG uptake and inflammation. Inflammation results in the release of enzymes capable of remodeling the extracellular matrix. The role of proteases and collagenases and their necessity for producing the disease pathology typically observed in tuberculosis has previously been reported [2, 4, 5].

It is important to note that increasing uptake of [^{18}F]-FDG was observed during disease progression, consistent with findings from recent studies [12–14]. These studies established that [^{18}F]-FDG uptake is correlated with CFU burden. While it has been reported that cavities provide an environment for high bacterial burden, it is unknown whether a high bacterial burden is a necessary prerequisite for cavitary formation [2, 8, 15]. It is plausible that the CFU burden prior to cavitation was similar between cavitary and noncavitary groups, and therefore there was a similar uptake of [^{18}F]-FDG. The density region that we observed to be increased during the course of disease progression was also independently reported in a marmoset model recently published by Via et al [12]. This suggests that the density region that we identified in this study may be applicable in model animals other than rabbits.

Limitations of the proposed study were that the predictive power of the algorithm is only 1 week at present. Lin et al [14] reported a similar lung density increase in *M. tuberculosis*–infected nonhuman primates. While we are optimistic that our algorithm can be extended to other species beyond rabbits, this has not been demonstrated. Noninvasive tests, such as sputum smear microscopy, interferon-γ release assays, and quantification of lung matrix and break down products, could be integrated into a multi-biomarker disease activity (MBDA) matrix for risk assessment. Similar approaches have been done for rheumatoid arthritis. This tool could be used to advance the understanding of cavity lesion development by identifying precavitary lesions.

Supplementary Data

Supplementary materials are available at *The Journal of Infectious Diseases* online (http://jid.oxfordjournals.org). Supplementary materials consist of data provided by the author that are published to benefit the reader. The posted materials are not copyedited. The contents of all supplementary data are the sole responsibility of the authors. Questions or messages regarding errors should be addressed to the author.

Notes

Acknowledgments. B. L., A. K., and W. R. B. designed the study. B. L., A. K., C. L., B. F., and U. B. generated the data. B. L., A. K., C. L., and W. R. B. wrote the first draft. B. L., A. K., C. L., B. F., U. B., D. J. M., S. J., and W. R. B. analyzed the data and revised the manuscript.

Financial support. This work was supported by the Swedish Research Council, the Swedish Society for Medical Research, the National Institute of Allergy and Infectious Diseases (grant RO1AI079590), the National Institutes of Health (grant RO1A1035272), and the Howard Hughes Medical Institute.

Potential conflicts of interest. All authors: No reported conflicts.

All authors have submitted the ICMJE Form for Disclosure of Potential Conflicts of Interest. Conflicts that the editors consider relevant to the content of the manuscript have been disclosed.

References

1. Global tuberculosis report 2012. Geneva, Switzerland: World Health Organization, **2012**.
2. Dannenberg AM. Pathogenesis of human pulmonary tuberculosis: insights from the rabbit model. Washington DC: ASM Press, **2006**.
3. Erkens CGM, Kamphorst M, Abubakar I, et al. Tuberculosis contact investigation in low prevalence countries: a European consensus. Eur Respir J **2010**; 36:925–49.
4. Elkington PT, D'Armiento JM, Friedland JS. Tuberculosis immunopathology: the neglected role of extracellular matrix destruction. Sci Transl Med **2011**; 3:71ps6.
5. Elkington P, Shiomi T, Breen R, et al. MMP-1 drives immunopathology in human tuberculosis and transgenic mice. J Clin Invest **2011**; 121:1827–33.
6. Blumberg HM, Burman WJ, Chaisson RE, et al. American Thoracic Society/Centers for Disease Control and Prevention/Infectious Diseases Society of America: treatment of tuberculosis. Am J Respir Crit Care Med **2003**; 167:603–62.
7. Wallis RS, Pai M, Menzies D, et al. Biomarkers and diagnostics for tuberculosis: progress, needs, and translation into practice. Lancet **2010**; 375:1920–37.
8. Nedeltchev GG, Raghunand TR, Jassal MS, Lun S, Cheng Q-J, Bishai WR. Extrapulmonary dissemination of *Mycobacterium bovis* but not *Mycobacterium tuberculosis* in a bronchoscopic rabbit model of cavitary tuberculosis. Infect Immun **2009**; 77:598–603.
9. Bagci U, Yao J, Miller-Jaster K, Chen X, Mollura DJ. Predicting future morphological changes of lesions from radiotracer uptake in 18F-FDG-PET images. PLoS One **2013**; 8:e57105.
10. Foster B, Bagci U, Luna B, et al. Robust segmentation and accurate target definition for positron emission tomography images using affinity

propagation. In: 2013 IEEE 10th International Symposium on Biomedical Imaging. New York: IEEE; **2013**;1461–4.
11. Bagci U, Udupa JK, Yao J, Mollura DJ. Co-segmentation of functional and anatomical images. Med Image Comput Comput Assist Interv **2012**; 15(Pt 3):459–67.
12. Via LE, Weiner DM, Schimel D, et al. Differential virulence and disease progression following Mycobacterium tuberculosis complex infection of the common marmoset (Callithrix jacchus). Infect Immun **2013**; 81:2909–19.
13. Davis SL, Nuermberger EL, Um PK, et al. Noninvasive pulmonary [18F]-2-fluoro-deoxy-D-glucose positron emission tomography correlates with bactericidal activity of tuberculosis drug treatment. Antimicrob Agents Chemother **2009**; 53:4879–84.
14. Lin PL, Coleman T, Carney JPJ, et al. Radiologic responses in cynomolgous macaques for assessing tuberculosis chemotherapy regimens. Antimicrob Agents Chemother **2013**; 57:4237–44.
15. Subbian S, Tsenova L, Yang G, et al. Chronic pulmonary cavitary tuberculosis in rabbits: a failed host immune response. Open Biol **2011**; 1:110016.